An Association of solar wind Energy Dynamics with polar Cap Potential and Field Aligned Current during Major Intense Geomagnetic Storms of Solar Cycles 22, 23 and 24

[1]Prashant Poudel, [2]Roshan Kumar Mishra, [1,2]Binod Adhikari
Department of Physics, Patan Multiple College, Tribhuwan University, Nepal
Department of Physics, St. Xavier's College, Kathmandu, Nepal

Corresponding Author: binod.adhi@gmail.com

Abstract

Invasion of solar wind particles inside earth's magnetosphere induces the distortion of geomagnetic setting of earth. This geomagnetic disturbances be a consequence of energy discharge of solar plasma in different forms such as visible aurora in the polar region, joule heating, ring current energy; momentary fluctuation of earth's magnetic field (SYM-H), intensification of magnetospheric current system; Field Aligned Current (FAC) and Polar Cap Potential (PCV) and many other phenomena. However, this event can cause some serious calamites, so having better understanding of it and able to be prepared in any severity of such situations is always in good accord. For this, we studied total of nine different intense geomagnetic storms from solar cycle 22, 23 and 24. Events included from solar cycle 22 and 24 were triggered by Stream Interaction Region (SIR) as well as SIR associated with complex structures which were a resultant of interactions between SIRs and Interplanetary Coronal Mass Ejections (ICMEs) respectively. The rest of the selected events which are all from solar cycle 23 were also the responses of solar structures like SIR and ICME along with sheath and magnetic cloud. To understand the impact of the solar wind particles on near earth space, magnetospheric and interplanetary parameters such as IMF-Bz, SYM-H, PCV and FAC are graphed along with total solar input energy and other energy sinks like auroral precipitation, joule heating, and ring current energy. To substantiate result, cross-correlation technique is used along with pie chart and bar graphing which has helped in statistical investigation. This techniques aided us in finding out that less than 1% of total solar input was contributed in ring current injection, joule heating and auroral precipitation combined. Solar Quiet (Sq) and Lunar (L) current was recorded to be playing the role of IMF-Bz to create disturbance as the plot showed the geomagnetic activity even in the absence of southward IMF-Bz. Mostly, the solar wind particles during intense storm was found to induce more intense eastward electrojet currents compared to ring current and westward electrojet current.

Key Words: Geomagnetic Storms, Solar Wind Energy, Joule Heating, Auroral Precipitation, Ring Current, Field aligned current and Polar cap potential

1. Introduction

The change in the geomagnetic setting of magnetospheric environment with the invasion of solar wind particles during geomagnetic disturbance is not an alien observation in near-Earth space science (Poudel et al, 2019). Solar wind is basically a stream of charged particles ignited from extremely hot corona in Sun (Parker, 1958). The Earth's dipole interacts with the magnetic field

possessed by the solar wind plasma ejected form upper part of the atmosphere of Sun (Adhikari and Chapagain, 2015) as a result energy is loaded into the different region of magnetosphere via global convection enhancing convection currents (Sergeev et al., 1995). These currents lead to deposition of energy in different forms such as ring current energy, joule heating, and auroral precipitation. Ring current energy is the energy associated with the kinetics of trapped solar wind particles that undergoes gyration and azimuthal drift motion along the field lines. This current is responsible for slight reduction of geomagnetic field in equatorial region and is equivalent to the number of charged particles in Van Allen radiation belt. Joule heating induces the ionospheric currents that heat the atmosphere and takes place through the Pedersen currents associated with the closure of field aligned currents in the resistive ionosphere (Koskinen and Tanskanen, 2002). This can be recognized as the frictional heating from the relative motion of plasma and neutrals [Song et al., 2009].

Auroral particle precipitation produces diverse forms of optical airglow caused by magnetospheric particles hitting the upper atmosphere (Newell et al. 2016). It is an important loss mechanism for plasma-sheet electrons and the precipitation produces important changes in the electrical conductivity of the ionosphere (Borovsky, 2018). Among the different types of magnetospheric current system flowing around the earth' surrounding, field-aligned current is one of them, which were first proposed by Birkland (1908). This current connects two regions: magnetosphere and ionosphere, by flowing along magnetic field lines but they are difficult to measure as this current have low current density (Milan et al, 2017; Adhikari and Chapagain, 2016). Dungey (1961) gave a model that discussed the interaction among several currents located in the ionosphere in low altitude, and how they couple with the magnetosphere through field-aligned currents (FACs). The reason for the existence of these currents is that the resistive behavior of the ionosphere requires FACs to close the divergence of the current density. During geomagnetic disturbance, the current systems existing inside the magnetosphere and ionosphere will be intensified [Jankovicova et al., 2002] and there is dawn-dusk asymmetry in the large-scale FACs [Anderson et al., 2005].

Polar cap potential (PCV) is the difference between the maximum and minimum values of ionospheric electric potential due to convection (Shepherd, 2006). During the solar-wind magnetosphere interaction, certain electric field is transferred to the polar ionosphere. This leads to creation of a potential difference in the ionosphere region and is referred to as cross PCV (Papitashvili et al., 1999; Pedatella et al., 2011). PCV is an important parameter used for determining what kind of interaction takes place between solar wind and magnetosphere. It is the manifestation of convection which results in creation of regions with maximum and minimum ionospheric electric potential (Shepherd, 2006). The increase in magnitude of IMF-B_z causes electric field of cross magnetosphere to increase, and it leads to increase in magnitude of ionospheric cross PCV (Adhikari and Chapagain, 2016).

In this paper, we aim to study the relation of Filed Aligned Current (FAC), Polar Cap Potential (PCV) and IMF-Bz with different magnetospheric energy such as ring current, joule heating and auroral precipitation. We will also provide the statistical analysis of the deposited energy, compare the major source of deposited energy into the magnetosphere and elaborate their nature

and also their relation with the other geomagnetic parameters with the backing of data evidence that supports our assumption.

2. Data Set and Methodology

We have considered nine events of different nature and intensity. We have taken comparative analysis method for the study. For the proper understanding of energy dynamics, potential and current system in the magnetosphere, we have considered solar wind energy (Utot), ring current energy (Ur), auroral precipitation (Ua), and joule heating (Uj), Polar cap potential (PCV) and filed aligned current (FAC). We have also applied cross-correlation technique to elaborate the relation between component of IMF (Bz) against Ur, Uj, Utot, Ua, and SYM-H, and the energy transfer mechanism. This technique helps to quantify the correlation and time lag between the already mentioned parameters which give us the time response of the process. The data needed for the analysis of these five events are extracted from Operating Mission as Nodes on the Internet web system.

Various methods have been suggested till now to study and quantify the relationship between the solar wind and magnetospheric response and also to forecast the geomagnetic activity based on the observed data of solar wind and IMF (Adhikari et al., 2018; Usoro, 2015; Wu & Lundstedt, 1997). To understand the magnetospheric response to the invading solar wind particles, various statistical method can be executed such as multiple regression, cross correlation, and visual correlation are useful methods according to review work of Baker et al. (1986). In this work, we have applied cross-correlation analysis method. The best-known method for correlative study is Pearson's correlation coefficient (r). The correlation coefficient ranges from −1 to +1, where value around zero means poor fit and positive and negative value depicts good linear fit. IMF-Bz, SYM-H, Utot, Ur and Uj, and Ua are the parameters included for the analysis. This technique compares and evaluates the information between two time series of the included parameters as a function of a time lag (Finch & Lockwood, 2007; Mannucci et al., 2008).

Table 1: Selection of geomagnetic disturbance events

Events	Date	Type	Solar Cycle	SYM-H
Event-1	1995 04 06-08	Intense	22	-163
Event-2	1998 09 24-25	Intense	23	-217
Event-3	1999 10 21-22	Intense	23	-228
Event-4	2000 09 17-18	Intense	23	-203
Event-5	2001 03 31 to 2001-04-02	Intense	23	-437
Event-6	2003 11 20-22	Intense	23	-490
Event-7	2004 11 07-09	Intense	23	-394
Event-8	2005 05 15	Intense	23	-305
Event-9	2015 03 17-18	Intense	24	-234

To calculate FAC and PCV, we apply formula suggested by Adhikari et al., (2017)

$$FAC = 0.328\left[n_p^{\frac{1}{2}} V_{sw} B_T Sin\frac{\theta}{2}\right]^{\frac{1}{2}} + 1.4\ [\frac{\mu A}{m^2}]$$

$$PCV = V_{sw} B_T Sin^2\frac{\theta}{2} \times 7R_e\ [kV]$$

Where, Solar wind density (n_p) is in n/cc, solar wind speed (V_{sw}) is in km/s, R_e is radius of Earth (6.38×10^6 m), B_T is total interplanetary magnetic field in nT; $B_T = \sqrt{B_y^2 + B_z^2}$ and angle of magnetic field (θ);

$$If\ B_Z > 0 \rightarrow \theta = \tan^{-1}(abs(\frac{B_y}{B_Z}))$$

$$If\ B_Z < 0 \rightarrow \theta = 180 - \tan^{-1}(abs(\frac{B_y}{B_Z}))$$

The total energy input to the magnetosphere (U_{tot}) is calculated by formula suggested by de Lucas et al., (2007)

$$W_\varepsilon = \int_{t_o}^{t_m} \varepsilon\, dt \text{ [J] and } \varepsilon = 10^7 V_{sw} B^2 l_o^2 Sin^4(\frac{\theta}{2}) \text{ [W]},$$

Where, B is IMF strength, θ is angle of magnetic field, $l_o = 7R_E$ is empirically determined factor. W_ε is obtained by integrating ε over the main phase from t_o to t_m of each magnetic storm. For the calculation of total energy input, all parameters are in SI unit.

Joule's heating (U_J) is given by.

$$U_J = (0.54 \times AE + 1.8) \times 10^9 \text{ [W]},$$

where, Auroral Electrojet (AE) index is in nT.

Auroral Precipitation (U_a) is given by

$$U_a = \left(4.4 \times \sqrt{abs(AL)} - 7.6\right) \times 10^9 \text{ [W]},$$

where, Amplitude Lower (AL) index is in nT.

Ring Current Energy (U_r) is given by

$$U_r = 4 \times 10^4 \left[abs\left(\frac{\Delta SYM-H}{60}\right) + abs\left(\frac{SYM-H}{4*60*60}\right)\right] \times 10^9 \text{ [W]},$$

where, ΔSYM-H = SYM-H(i+1) – SYM-H(i) and SYM-H is in nT.

3. Result and Discussion

Figure **1** is the graphical representation of dynamics of the energy sinks (Ua, Uj, Ur and Usw) along with the variation of SYM-H, IMF-Bz, FAC and PCV during the intense storm of Oct 22, 1999. This was one of the intense storm events during solar cycle 23. This event was triggered by SIR associated with complex structures due to interactions between SIRs and Interplanetary Coronal Mass Ejections (ICMEs) respectively and has already been studied by Dal Lago et al. (2006). Observations of this event from WIND satellite exhibit obvious signatures of an ICME. This event was also listed in Jian's ICME catalog (Jian et al., 2006), Richardson and Cane's ICME catalog (Richardson & Cane, 2010), and USTC's ICME catalog (Chi et al., 2016). As observed in the figure, the first day of this event (21st October) has smooth SYM-H value with not much fluctuation. However, after couple of hours, we can observe slightly positive rise in SYM-H value which was accompanied by definite fluctuation in geomagnetic parameters PCV and FAC along with IMF-Bz. Interestingly, the orientation of IMF-Bz is mostly northward during this time. Obviously, it is evident that this activity was happening inside the magnetosphere without geomagnetic reconnection between IMF and magnetosphere.

After observing the nature of the initial phase of the disturbance, the event could be identified as SC (Sudden Commencement) or SSC (Storm Sudden Commencement). SSC events occur due to a rapid compression in the Earth's magnetic field which is generally believed to be caused by Interplanetary (IP) shocks, but with a few exceptions. Park et al (**2015),** investigated 274 geomagnetic storms and proposed an idea that that HSSs (High Speed Streams) and ICMEs may be alternative contributors to SSCs. Interestingly, FAC, PCV and energy sinks (Ua and Uj) related to the polar part of the ionosphere was active, but little to none action was sensed in the ring current.. Normally after reconnection, solar particles are dragged along with the broken-field lines and are stored on the magneto tail which later gets loaded into night side inducing ring current.

As the magnetic reconnection was absent, there was not enough ring current particles undergoing convection of plasma sheet into the inner magnetosphere and eventually no depression of SYM-H value. Later, at the end of the first day of the event, geomagnetic storm was observed. Sudden southward change of IMF-Bz was accompanied by abrupt change in Ua, Ur, PCV and FAC. As storm moved onto main phase, ring current injection was increasing almost linearly unlike other energy sinks which were more chaotic.

Uj and Ua both attained their maximum value of the event of 7.7886 $\times 10^{11}$ Watt and 1.6281×10^{11} Watt respectively during this phase. As the main phase was progressing into the recovery phase, there was delay in decreasing value of FAC, PCV and Ur compared to Uj and

Ua. Around the end of the main phase, there was big flux of solar wind interacting with magnetosphere. But as the direction of the wind was approaching northward, hardly any activity was seen in the value of FAC, PCV, Ua and Ur. Opposite polarity of magnetopause screened the invading solar particles to penetrate through the field lines along with the load of the energy in the polar part of magnetosphere system. However, Ur kept increasing its value and showed only a slight spike during this time. This could be due to presence of enough ring current particles induced during main phase that endured SYM-H value depression. But the density of these energetic particles slowly started decreasing as the storm went into the recovery phase and all the parameters started regaining its pre storm value. The recovery is associated with a multitude of physical processes associated with the loss of the energetic ring current particles such as charge exchange, Coulomb collisions, wave–particle interactions and convection on the dayside magnetopause (West et al., 1972; Kozyra et al., 1997, 2006a; Jordanova et al., 1998; Daglis et al., 1999).

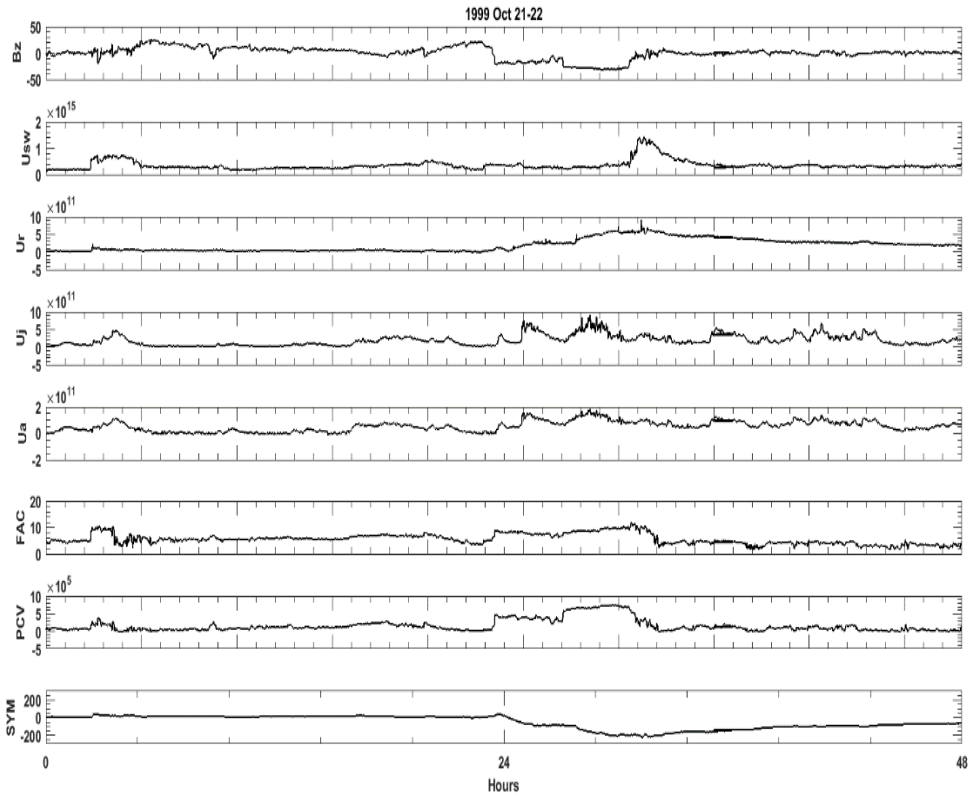

Figure 1: From top to bottom, the panels show the variations of IMF-Bz (nT), solar wind energy (Utot in Watt), ring current energy (Ur in Watt), Joule heating (Uj in Watt), Auroral precipitation (Ua in Watt) with time (hours), Field Aligned Current (μAm^{-2}), Polar Cap Potential (kV) and SYM H = symmetric horizontal component of geomagnetic field respectively, for the event-3 of Oct 22, 1999.

(a)

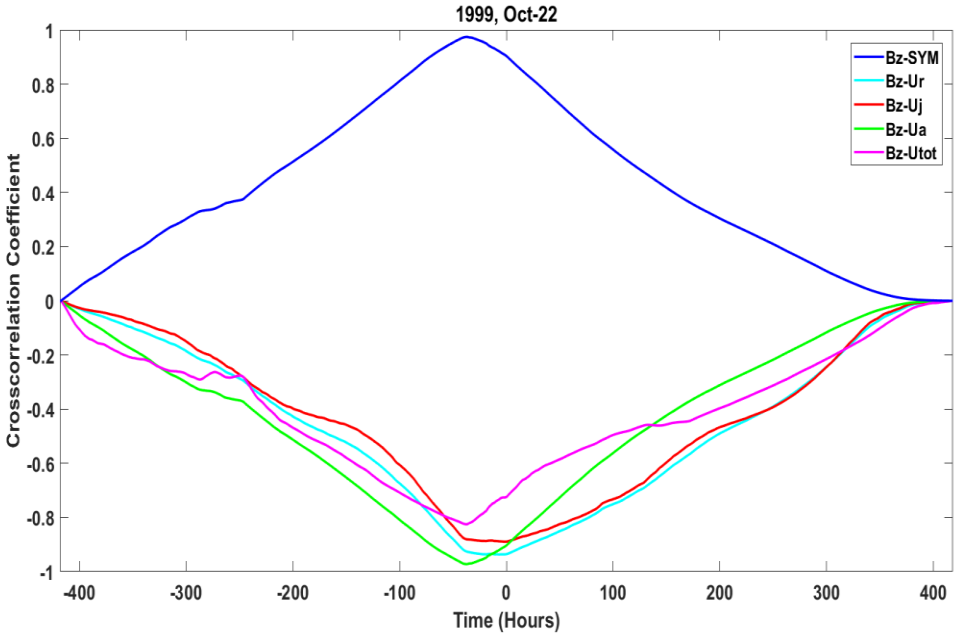

(b)

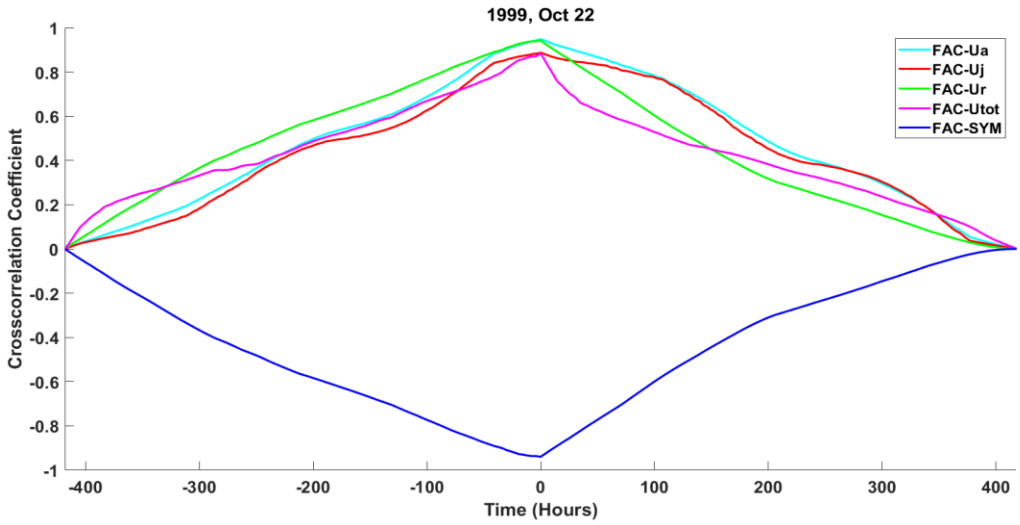

211

212

213

214

215

216

217

218 **(c)**

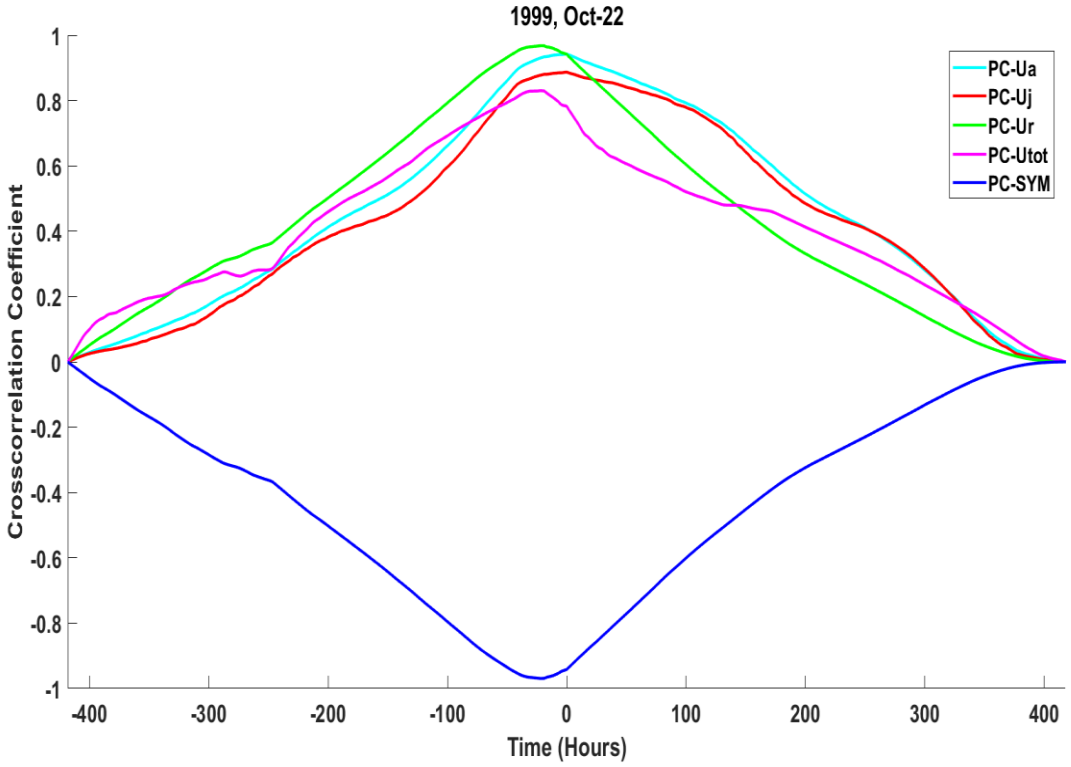

Figure 2: Cross correlation of SYM-H (nT), Uj (Watt), Ur (Watt), Ua (Watt), Utot (Watt) during 1999, Oct 22 with: (a) Southward component of IMF, Bz (nT), (b) Filed Aligned Current (μAm^{-2}) and (c) Polar cap potential (kV).

Figure **2.a** delineates the cross-correlation results of SYM-H, Uj, Ur, Ua, Utot with IMF-Bz during 1999, Oct 22. The horizontal axis represents the scale in minutes (ranging from −420 minutes to 420 minutes) and the vertical axis represents the coefficient of cross correlation. Here, the positive correlation is shown by IMF-Bz-SYM-H pair and the rest of the pair is negatively correlated. Positive cross correlation between IMF-Bz and SYM-H is obvious due to the direct proportional relation between them i.e. negative value of IMF-Bz (southward orientation) triggers the depression of SYM-H value. The maximum correlation coefficient between the IMF-Bz and SYM-H is 0.9743 at time lag -37 min. This result is in agreement with Bargatze et al. (**1999**) and Rostoker et al. (**1972**) where they studied substorm and concluded that the time delay between solar wind energy input and the release of energy in the magnetotail is considerably longer, of the order of 30–60 min. Out of all the nine intense storm events considered, this event (event-3) has highest cross correlation coefficient for IMF-Bz - SYM-H pair. This correlation coefficient value is even higher than that observed by Poudel et al. (2019) where the coefficient value was 0.9297 with time lag of -170 min. Such higher magnitude of correlation coefficient might have occurred due to the significant role played by IMF-Bz for the injection of energetic particles in this particular event, even though IMF-Bz is not sufficient condition for triggering of geomagnetic storm in most of the cases (Poudel et al, 2019).

A sufficiently large IMF-Bz might be adequate to create geomagnetic disturbance as stated by Gonzalez et al. (1994) and Gonzalez and Tsurutani (1987). IMF-Bz correlates negatively with rest of the parameters because of inverse proportionality of IMF-Bz. This means decrease in IMF-Bz value (southward orientation) would increase the value of solar wind input energy, dissipated energy in coupled magnetosphere-ionosphere, intensity of magnetospheric current and potentials at the polar cap. IMF-Bz correlation coefficient with Uj is -0.8896 at time lag −1 min; with Ua is -0.9725 at time lag −37 min; with Ur is -0.9365 at time lag −6 min and with Utot is -0.8252 at time lag −38 min. The time lag for all the pairs for this event was also observed to be negative i.e. IMF-Bz was ahead of all other variables (FAC, PCV, Ua, Ur, Uj and Utot) intimating that the response of IMF-Bz was first observed in the station and then on other activities of the magnetosphere.

Figure **2.b** delineates the cross-correlation results of SYM-H, Uj, Ur, Ua, Utot with FAC during 1999, Oct 22. Here, the time scale represented by x axis ranges from −420 to 420 minutes and y axis representing the coefficient scale ranges from −1 to 1. At this point, the negative correlation is shown by FAC-SYM-H pair and the rest of the pair shows positive correlation. FAC correlating positively with the SYM-H makes sense as the increase in intensity of solar particles moving along the geomagnetic field lines from magnetopause and loading off to polar region would lower the SYM-H value i.e. increase in FAC triggers the depression of SYM-H value. And the negative correlation of FAC with the rest of the variables signifies that convection of field aligned current particles would assist in the increasing the energy sinks in magnetosphere and increases the differences of ionospheric electric potential. FAC correlates at zero-time lag with all three magnetospheric energy sinks, invading solar energy and SYM-H i.e they are in same phase at their respective highest coefficient. This means that the response observed for all the variables corresponding to FAC was same without any delay or lead.

Comparing the coefficient value, FAC correlated highly with Ua with (0.9487) and least with Utot (0.8837). Similarly, FAC showed correlation coefficient of 0.9429 with Ur, 0.8872 with Uj and -0.9399 with SYM-H. The result obtained by Adhikari et al (2018) for the correlation of FAC-SYM-H pair was same regarding the time lag (0 minutes) but had highest coefficient value of 1. As explained by Adhikari et al (2018), the coefficient for FAC-SYM-H pair is the highest when the ring current energy is the dominant which makes sense as joule heating instead of ring current was the highest for our result. Numerically, joule heating and auroral precipitation is function of AE. So, whenever, value of AE intensifies so would happen to joule heating and aurora precipitation. And as suggested by Wei et al. (2008), during late main phase and early recovery phase, the FAC is directly proportional to *AE*. That means, increase in FAC would eventually help to increase the energy sink of joule heating auroral precipitation and was really the case in our results as well.

Figure **2.c** delineates the cross-correlation results of SYM-H, Uj, Ur, Ua, Utot with PCV during 1999, Oct 22. The horizontal axis represents the scale in minutes and the vertical axis represents the cross correlation coefficient. In this figure, the scales of −500, −400, −300, −200, −100, 0, 100, 200, 300, 400 and 500 are labeled in the horizontal axis and cross-correlation coefficient runs to its range in the vertical axis. Like the nature of correlation plot of FAC; PCV also correlates negatively with SYM-H and positively with the rest of the variables. This is caused by

the increase in ionospheric potential due to the convection of energetic particles at the time of magnetic storm. SYM-H value thereby would depress and increase the energy deposition in different parts of magnetosphere. PCV was found to be in phase (zero-time lag) with Ua and Uj with cross correlation coefficient of 0.9425 and 0.887 respectively. PCV showed good correlation with Ur but little delayed response (time lag -19 minutes). However, PCV had comparatively less correlation with total solar input energy (Utot). Their cross correlation coefficient was 0.8301 at time lag of -22 minutes. This confirms, highly energetic solar flux does not ensure would have similar influence on polar cap potential. Similarly, PCV showed strong correlation with coefficient value of 0.9679 with Ur and -0.9693 with SYM-H with time lag of -19 minutes and -20 minutes, respectively.

Similar statistical analysis is carried out for the other remaining eight intense storms as well. The discussion of energy panels along with cross correlation plots for all of the events are summarized in the Table **2**, **3 and 4.** This particular event was included for the explanation, as the parameters of invading solar wind particles had good correlation with geomagnetic variables. Along with that, the nature of energy dynamics also showed some interesting and unique characteristics that was very necessary for the elucidation.

Percentage energy composition inside magnetosphere

Here, figure **3** represents the percentage composition of the energy deposited inside the magnetosphere during main phase of all the nine intense storms included in this research. Ring current energy (Ur), joule heating (Uj) and auroral precipitation (Ua) are considered for the analysis. As observed in the chart above, out of nine intense storms, six storms had joule heating as the major energy sink whereas during remaining three events, ring current energy was the dominant one. Auroral precipitation was the weakest during all the nine events. Akasofu (1978) believed that ~90% of energy dissipation for geomagnetic storm would be through ring current injection. Later work of Knipp et al. (1998) and Turner et al. (2009) found out that joule heating dominates over other form of magnetospheric energy sinks as dissipation channel during storm events (Poudel et al, 2019). Tenfjord and Ostgaard (2013) also studied different periods and events of different durations and showed joule heating as the major energy compared to ring current injection and auroral precipitation. However, they did mention that the calculation does deviates depending upon the type of coupling function used. They claimed that the coupling function, P_{storm} (as represented in their work) which was used in their study is more essential and performs better than the ε parameter scaled to the energy sink.

Event **5**, **7** and **8** stored majority of energy for the kinetics of the ring current particles. SYM-H depression were significantly high during these three events. Pulkkinen et al, (2001) claimed that the average ring current energy contributes more than 50% of the SYM-H depression. Therefore, events with intense SYM-H depression events can be expected to contribute major percentage of energy to the ring current energy sink. Auroral precipitation contributing least to the energy sink of magnetosphere was the common situation in all nine cases. In this paper we estimated the Auroral precipitation and Joule heating using AL and AE indices as a proxy. AE index mathematically is the difference of the value of AL and AU. Indices AL and AU represents eastward and westward electrojet currents. As observed from the chart representation, joule

heating was major sink and auroral precipitation was on the minority, it is conformed that the solar wind particles during intense storm produces electrojet currents more on the eastward than westward.

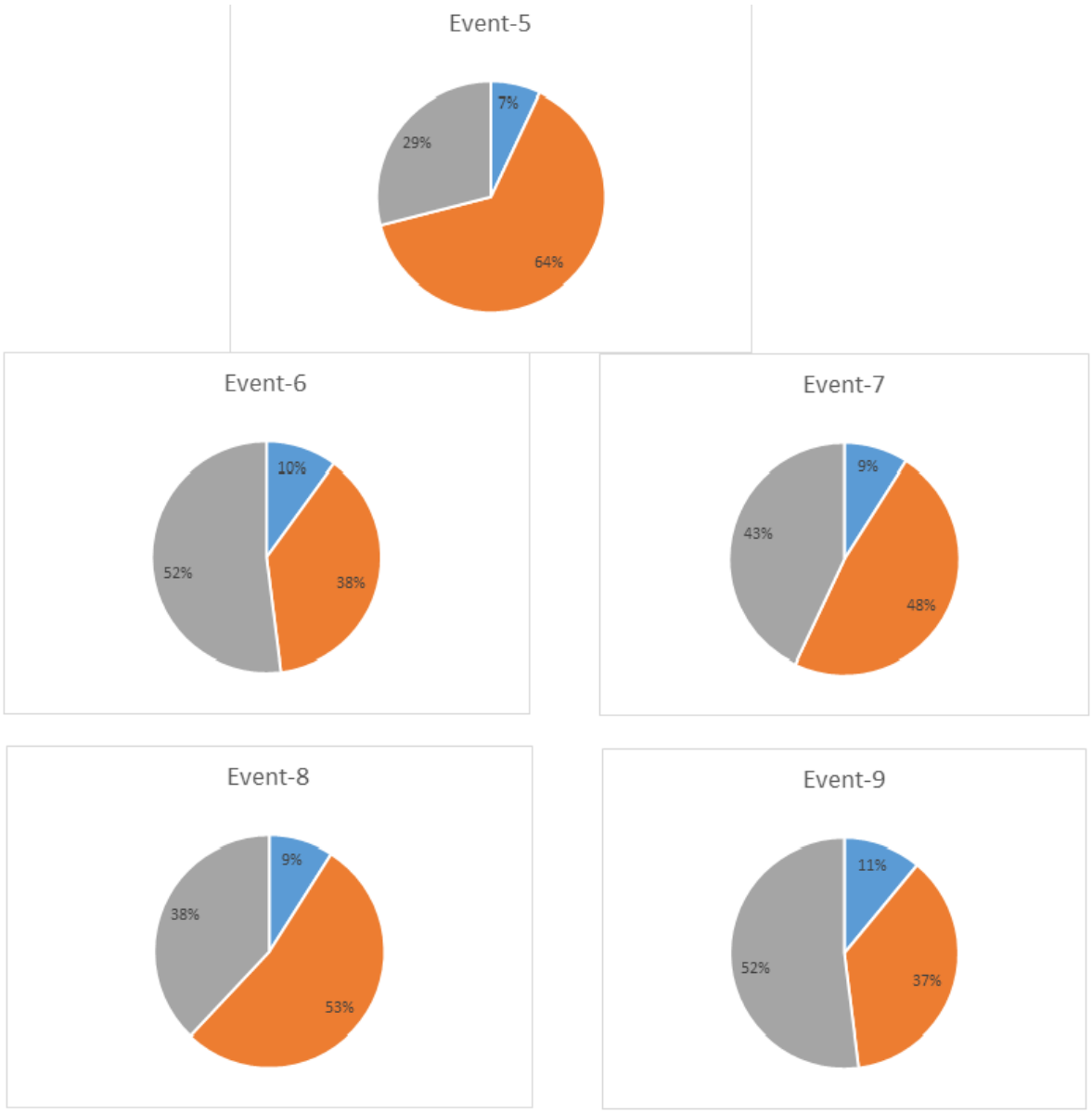

Figure 3: Percentage compositions of magnetospheric energy sinks during intense geomagnetic storm: (a) Event-1, (b) Event-2, (c) Event-3, (d) Event-4, (e) Event-5, (f) Event-6, (g) Event-7, (h) Event-8 and (i) Event-9.

Comparison of percentage dissipation of total solar energy input

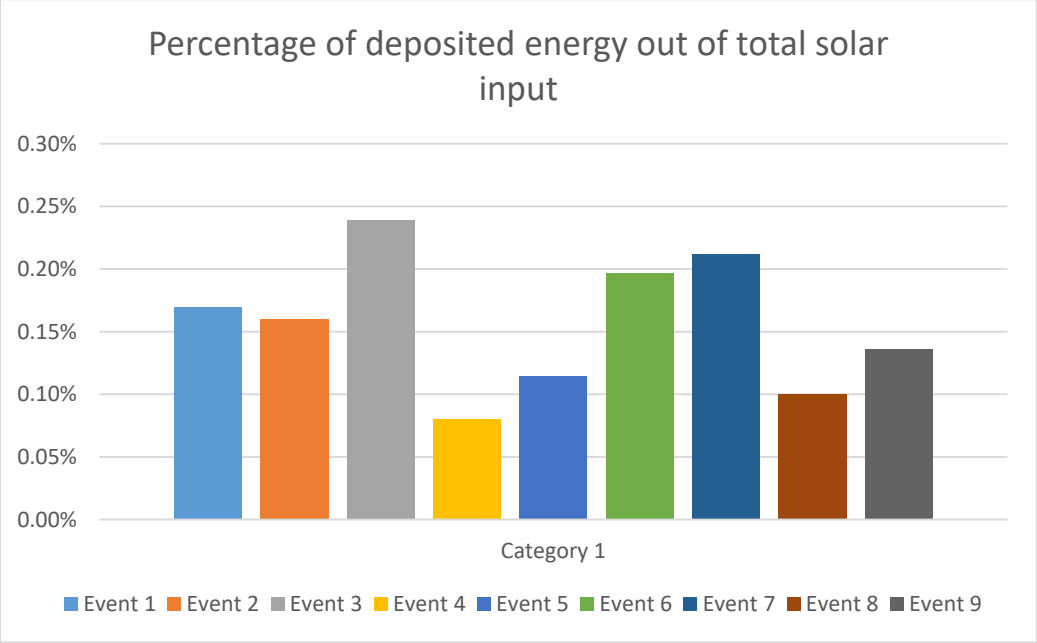

Figure 4: Bar graph representing the percentage of total energy decomposition of total soar input

Figure 4 delineates the bar graph of total deposited energy (Ua, Uj and Ur combined) for main phase of the nine selected intense geomagnetic storms. Very less portion of total solar input seemed to be dissipated inside the magnetosphere. All the nine events had deposition of less than 1 % of the total solar input. This observation aggresses with the studies done by Østgaard et al. [2002b] and Stern [1984] where they found out that the efficiency of solar wind energy deposited into the magnetosphere is smaller or roughly ≈ 1%. Østgaard et al. [2002b] discussed about an important parameter called the coupling efficiency, which is how much of the available solar wind kinetic energy that penetrates the magnetosphere. They investigated the data from the period 1997–2010 and found out that the efficiency on average is 0.8%. Similarly, Stern [1984] estimated it to be around 1% but Lu et al. [1998] suggested little higher with the value to be as much as 4%. This is because most of the energy of the solar wind particles is not stored inside the magnetosphere but gets ejected down the magnetotail to be lost from the Earth to the space, the process called plasmoid ejection. As observed in the graph, out of all nine events, event 3rd (Oct 22, 1999) deposited highest percentage (0.24%) of energy into the magnetosphere and event

4^{th} (Sep 17-18, 2000) was the lowest of the nine with one third of the energy deposited during event 3^{rd} (0.08%).

Table 2: Total and average deposited magnetospheric energy

Events	Ur		Uj		Ua		Utot	
	Total	Average	Total	Average	Total	Average	Total	Average
1	1.6138×10^{14}	1.8235×10^{11}	3.1715×10^{14}	3.5836×10^{11}	7.3101×10^{13}	8.2600×10^{10}	3.1863×10^{17}	3.6003×10^{14}
2	1.4125×10^{14}	3.7468×10^{11}	1.7205×10^{14}	4.5637×10^{11}	3.7785×10^{13}	1.0022×10^{11}	2.1352×10^{17}	5.6636×10^{14}
3	1.5231×10^{14}	3.6437×10^{11}	1.5651×10^{14}	3.7442×10^{11}	4.3101×10^{13}	1.0311×10^{11}	1.4898×10^{17}	3.5642×10^{14}
4	8.1808×10^{13}	3.4373×10^{11}	1.0769×10^{14}	4.5248×10^{11}	2.5415×10^{13}	1.0679×10^{11}	2.6851×10^{17}	1.1282×10^{15}
5	1.5897×10^{14}	7.8698×10^{11}	7.3533×10^{13}	3.6402×10^{11}	1.7282×10^{13}	8.5556×10^{10}	2.1728×10^{17}	1.0757×10^{15}
6	2.9636×10^{14}	4.8985×10^{11}	4.0642e+14	6.7176×10^{11}	7.9847×10^{13}	1.3198×10^{11}	3.8723×10^{17}	6.4004×10^{14}
7	3.3594×10^{14}	6.1192×10^{11}	2.9931×10^{14}	5.4518×10^{11}	6.6413×10^{13}	1.2097×10^{11}	3.2690×10^{17}	5.9545×10^{14}
8	8.0575×10^{13}	6.7710×10^{11}	5.8872×10^{13}	4.9472×10^{11}	1.3304×10^{13}	1.1180×10^{11}	3.2690×10^{17}	1.2649×10^{15}
9	3.0628×10^{14}	3.2071×10^{11}	4.3004×10^{14}	4.5030×10^{11}	9.1000×10^{13}	9.5288×10^{10}	6.0862×10^{17}	6.3730×10^{14}

Given table **2** summarizes the average and sum of all three deposited energy Ua. Ur and Uj including solar input Utot during main phase of all nine selected events. Here, energy is expressed in the units of Watt. Even though, event 3 had the highest total solar input to deposited magnetospheric energy conversion ratio, but event 8 was experiencing intense solar flux input of 1.2649×10^{15} Watt on average. Interestingly, compared to other events of lesser solar input, this event (event 8) could not contribute at the highest level for any form of energy sinks. It comes second on ring current injection, third on joule heating and third on auroral precipitation. One of the reasons for such observation is, out of all nine-storm event, it had the shortest main phase duration. So, it got lesser time to inject energy inside the magnetosphere compared to others. Talking about highest energy sink, event-5 was the highest for ring current injection (7.8698×10^{11} Watt), event-6 was the highest for joule heating (6.7176×10^{11} Watt) and event-6 was the highest for auroral precipitation (1.3198×10^{11} Watt).

Table 3: Cross correlation coefficient and time lag of IMF-Bz vs SYM, Ua, Uj, Ur and Utot

	Bz-SYM		Bz- Ua		Bz-Uj		Bz-Ur		Bz-Utot	
Date	Coef	Time	Coef	Time	Coef	Time	Coef	Time	Coef	Time
Apr 7, 1995	0.8547	-66	-0.8535	-66	-0.7944	-7	-0.8158	-7	-0.8104	25
Sep 25, 1998	0.8378	-52	-0.8364	-50	-0.6892	-11	-0.7739	-28	-0.7985	33
Oct 22, 1999	0.9743	-37	-0.9725	-37	-0.8896	-1	-0.9365	-6	-0.8252	-38
Sep 17-18,	0.8245	-99	-0.809	-96	-0.7145	-24	-0.7398	-19	-0.6736	-2

2000										
Mar 31, 2001	0.9367	-11	-0.9412	-11	-0.8524	-5	-0.9309	-4	-0.8058	52
Nov 20, 2001	0.878	0	-0.8753	0	-0.7643	1	-0.8018	0	-0.7207	247
Nov7-8, 2004	0.9216	-43	-0.9221	-39	-0.8629	0	-0.9347	0	-0.8479	137
May 15, 2005	0.8746	-23	-0.8752	-6	-0.9524	0	-0.9702	0	-0.9676	0
Mar 17, 2015	0.8428	-11	-0.8452	-5	-0.8171	19	-0.8466	0	-0.8119	319

Given table **3** shows the correlation coefficient and time lag of magnetospheric parameter IMF-Bz with all three deposited energy Ua. Ur and Uj along with solar input Utot and SYM-H during main phase of all nine selected events. On comparing the events for IMF-Bz-SYM-H dynamics, event 3 had the highest correlation with time lag of -37 minutes. This means, SYM-H showed response 37 minutes later to fluctuation of invading IMF-Bz. Response of Ur for IMF-Bz was also good with -0.9365 and time lag -6 minutes which is the second highest correlation when compared to all other events. Ur was faster than SYM-H to show the reaction as it had lesser time delay. This makes sense as first ring current particles intensifies which later would depress the SYM-H value. This event also had the highest SYM-H-Ua correlation of all the events with -0.9725-time lag -37 minutes. Interestingly, compared to Ua; Uj showed weaker correlation of -0.8896 but at better time lag -of 1 minutes. This means Ua fluctuation was more like IMF-Bz than Uj but slower in response to the change in invading IMF-Bz.

Table 4: Cross correlation coefficient and time lag of FAC vs SYM, Ua, Uj, Ur and Utot

	FAC-SYM		FAC- Ua		FAC-Uj		FAC-Ur		FAC-Utot	
Date	Coef	Time	Coef	Time	Coef	Time	Coef	Time	Coef	Time
Apr 7, 1995	-0.9028	-74	0.9567	0	0.9357	0	0.9055	-73	0.9781	0
Sep 25, 1998	-0.8384	-21	0.9441	0	0.8965	0	0.8457	-20	0.9708	0
Oct 22, 1999	-0.9399	0	0.9487	0	0.8872	0	0.9429	0	0.8837	0
Sep 17-18, 2000	-0.8387	-60	0.9588	0	0.9369	0	0.84	-62	0.9613	0
Mar 31, 2001	-0.8958	-6	0.9528	0	0.9263	0	0.9042	-6	0.9275	0
Nov 20, 2001	0.845	-4	0.9602	0	0.9223	2	0.8546	-3	0.9082	0
Nov7-8, 2004	-0.8795	-68	0.9334	0	0.8958	0	0.884	-69	0.9535	0
May 15, 2005	-0.9327	-5	0.974	0	0.9437	0	0.9442	-3	0.9913	0
Mar 17, 2015	-0.8773	-87	0.9089	0	0.8818	0	0.8838	-64	0.9592	0

Given table **4** shows the correlation coefficient and time lag of magnetospheric parameter FAC with all three deposited energy Ua, Ur and Uj along with solar input Utot and SYM-H during main phase of all nine selected events. FAC was in good phase with all these energy sinks during every storm event studied here, as for most of them time lag was 0 minutes. Event 8 had good impact among all the events as it had the highest relation for all the energy sinks as well as SYM-H. FAV correlated with SYM-H, Ua, Ur, Uj and Utot with respective coefficient of -0.9327, 0.974, 0.9442, 0.9437 and 0.9913 respectively. Ua and Uj both being the function of auroral indices, was in phase with FAC but was ahead of SYM-H variation and Ur by 5 minutes and 3 minutes, respectively. Event 6 showed quite distinctive characteristics as FAC-Ur time lag was positive of two minutes. This result suggests that, there was some activity of joule heating happening already before FAC current. This means, ohmic dissipation in ionosphere is not only the consequences of field aligned current particles.

Table 5: Cross correlation coefficient and time lag of PCV vs SYM, Ua, Uj, Ur and Utot

	PC-SYM		PC- Ua		PC-Uj		PC-Ur		PC-Utot	
Date	Coef	Time	Coef	Time	Coef	Time	Coef	Time	Coef	Time
Apr 7, 1995	-0.9052	-66	0.8742	-6	0.8342	-7	0.9055	-66	0.9172	0
Sep 25, 1998	-0.8942	-52	0.8981	0	0.8281	0	0.8964	-49	0.9275	1
Oct 22, 1999	-0.9693	-21	0.9425	0	0.887	0	0.9679	-19	0.8301	-22
Sep 17-18, 2000	-0.8128	-96	0.8908	8	0.8781	0	0.8009	-96	0.8743	2
Mar 31, 2001	-0.9375	-10	0.9439	-3	0.8757	0	0.9423	-9	0.8229	7
Nov 20, 2001	-0.8781	-1	0.915	0	0.8748	1	0.8825	0	0.7522	10
Nov7-8, 2004	-0.9203	-65	0.9552	0	0.8975	0	0.9223	-47	0.8716	21
May 15, 2005	-0.9156	-8	0.9807	0	0.9516	0	0.9216	-6	0.9813	0
Mar 17, 2015	-0.8943	-30	0.9222	0	0.8947	-26	0.9006	-40	0.8732	51

Given table **5** shows the correlation coefficient and time lag of magnetospheric parameter PCV with all three deposited energy Ua, Ur and Uj along with Utot and SYM-H during main phase of all nine intense geomagnetic storms. PCV seems to have very good influence on the magnetopsheric energy sinks. We observed, event-3 had the highest average energy deposition but had unsubstantial impact in auroral dynamics compared to other eight events. It had the strongest correlation of -0.9693 and 0.9679 with SYM-H and Ur respectively. Even though having strong correlation coefficient manifested the similarity of their characteristics, there was still significant time delay between them. That means, potential was setup first in ionosphere and minutes later (21 for SYM-H and 19 for Ur) ring current induced and SYM-H activity started.

PCV had good influence on polar weather in event 8 as it had it's the highest correlation with Ua (0.9807) and Uj (0.9516) during this time. PCV was in phase (zero-time lag) with total solar input and strongly correlated with Utot (0.9813) as well. Like that by FAC, PCV also showed quite distinctive characteristics during event 6 storm as FAC-Uj time lag was positive one minute. This result hints us about the intensification of joule heating before PCV was active.

4. Summary

For the first time, this paper studies all the major intense storm included from solar cycle 22, 23 and 24 and provides the statistical analysis of the energy dynamics and current system of the magnetosphere during such events. Nine intense storms from 1995 to 2015 are analyzed using measurements from the OMNIWEB network of ground-based magnetometers. Various interplanetary and geomagnetic parameters were studied to understand the dynamics of the geomagnetism, current system and energy distribution inside the magnetosphere during geomagnetic disturbance. Different statistical analysis technique were executed to the parameters included in the research which helped us to dig out important information about magnetospheric dynamics of earth.

The highlights of the study can be summarized as follows:

- Events included from solar cycle 22 and 24 were triggered by Stream Interaction Region (SIR) as well as SIR associated with complex structures which were a resultant of interactions between SIRs and Interplanetary Coronal Mass Ejections (ICMEs) respectively. The rest of the selected events which are all from solar cycle 23 were also the responses of solar structures like SIR and ICME along with sheath and magnetic cloud.
- Comparing on the basis of time average of solar wind energy input, event 8 experienced the most (1.2649×10^{15} Watt) and the event 3 was the experiencing the least amount (3.5642×10^{14} Watt) of invading solar flux. However, highest average deposited energy inside the magnetosphere was during event 6 (Table **2**).
- Less than 0.5 % of total solar input was deposited inside the magnetosphere for all the nine intense storms. Maximum deposited energy was during event 3 with 0.24 % and the minimum was deposited during event 4 with 0.08% (Figure **4**).
- Joule heating, ring current injection and auroral precipitation was studied for the research. Out of these three energy sinks, joule heating turned out to be the dominant one for significantly number of times. Six times, joule heating contributed the most and during 5 of those 6 times, it was around 50% or more. Ring current energy was dominant for the rest of three events. Auroral precipitation was the weakest one during all nine events.
- Intensity of the solar cycle appeared to be swelling. 24 was the weakest one and 22 was the strongest one.
- IMF-Bz, FAC and PCV showed very strong correlation with all the deposited energies, total solar input and SYM-H.
- The inversely proportional relation between SYM-H index and ring current energy as proposed by Dessler Parker-Scopke relation holds true.
- Solar wind parameters IMF-Bz correlates positively with SYM-H and negatively with ring current energy (Ur), joule heating (Uj), auroral precipitation (Ua), and solar wind energy (Utot).

5. Conclusion

This study attempts to contribute on the understanding of the solar induced electromagnetic phenomena also known as geomagnetic storm; the influence of which has been observed in technological inventions for over a century. This paper has focused on the energy dynamics of invading solar wind energy input, deposited energy inside the magnetosphere-ionosphere couple and characteristics of magnetospheric current and potential system during highly intense solar storm period. Hence, the conclusion of this research work encompasses:

- Our result approved of the orientation of IMF-Bz playing significant role in letting the solar wind particles inside the magnetosphere. Be that as it may, some geomagnetic activity were observed irrespective of the orientation of IMF-Bz. This suggested that magnetic reconnection is important but not the singular reason for the geomagnetic disturbance. The viscous interaction of charged solar wind particles and the magnetopause, solar quiet, and lunar quiet current system could as well be the triggering factor for the disturbance.
- Joule heating turned out to be the major contributor as an energy sink inside magnetosphere during geomagnetic storm. Its impact on middle to low latitude ionosphere appeared quite evident. Radio wave signal distributed by man-made technology is spread throughout the ionosphere region. This indicates that the impact of joule heating on manmade technology is highly plausible.
- Undoubtedly, as observed from the result, joule heating was the dominant channel of solar wind energy transfer into the magnetosphere. This result was very consistent with many studies done by other researcher. Even though, ring current energy was considered to be the dominant one but every important study done in recent time's accounts joule heating as the main dissipation mechanism. This means that the energy deposition due to the increase in the electric conductivity within ionosphere during geomagnetic disturbance is more than the kinetics of the ring current particles encircling the equatorial plane of earth. Particles precipitation in the auroral region is observed visually as polar lights and is easy to measure using ultraviolet images but its energy contribution is still least of the three.
- Cross correlation coefficient was significantly strong for all the parameters. Specifically, high correlation of SYM-H, Ua and Uj indicated strong coupling with magnetosphere and magnetosphere coupling with ionosphere.

As future perspectives, this paper will open so many prospects for further research associated with the space weather. Activities in the absence of magnetic reconnection implied that a study of the expanse of energy invaded inside magnetosphere through polar cusp can be conducted. Total energy deposited inside magnetosphere was calculated to be less than 0.5% of the total solar input. So, we can investigate whether the rest of the energy **is stored in tail of magnetosphere** or there are other forms of energy sinks yet to be considered. The disturbance that magnetosphere go through is just due to the energy sinks which turned out to be less than 0.5% of total solar input or other factors such as cosmic energetic ray play significant role.

Acknowledgments

The data sets for this study were obtained from the OMNI website (https://omniweb.gfsc.nasa.gov/). We sincerely acknowledge staff members from NASA.

References:

1. Poudel, P., Simkhada, S., Adhikari, B., Sharma, D. and Nakarmi, J. J. (2019). Variation of Solar Wind parameters along with the undersrnding of energy dynamics within the magnetopsheric system during geomagnetic disturbances. *Earth and Space Science*, **6**, 276-293.
2. Parker, E. N. (1958). Interaction of the solar wind with the geomagnetic field. *Physics of Fluids*, **1**, 171– 187.
3. Adhikari, B. and Chapagain, N. P. (2015). Polar cap potential and merging electric field during high intensity long duration continuous auroral activity. *Journal of Nepal Physical Society*, **3**, 6-17. Adhikari, B., Dahal, S., Sapkota, N., Baruwal, P., Bhattarai, B., Khanal, K., & Chapagain, N. P. (2018). Field-aligned current and polar cap potential and geomagnetic disturbances: A review of cross-correlation analysis. Earth and Space Science, 5, 440–455. https://doi.org/10.1029/2018EA000392.
4. de Lucas A., W. D. Gonzalez, E. Echer, F. L. Guarnieri, A. Dal Lago, M. R. da Silva, L. E. A. Vieira, N. J. Schuch (2007), Energy balance during intense and super-intense magnetic storms using an Akasofu ε parameter corrected by the solar wind dynamic pressure, Journal of Atmospheric and Solar-Terrestrial Physics, 69(5), 1851-1863, https://doi.org/10.1016/j.jastp.2007.09.001.
5. Sergeev, V. A., Pellinen, R. J., & Pulkkinen, T. I. (1995). Steady magnetospheric convection: A review of recent results. *Space Science Reviews*, **75**, 551– 604.
6. Koskinen, H. E. J. and Tanskanen, E. I. (2002). Magnetospheric energy budget and the epsilon parameter. *Earth and Space Science*, **107**, SMP 42-1-SMP 42-10.
7. Song, P., V. M. Vasyliūnas, and X.-Z. Zhou (2009), Magnetosphere-ionosphere/thermosphere coupling: Self-consistent solutions for a one- dimensional stratified ionosphere in three-fluid theory, *J. Geophys. Res.*, **114**.
8. Newell P. T., Liou K., Zhang Y., Sotirelis T. S., Paxton L. J., Mitchell E. J. (2016). Auroral precipitation models and space weather. Geophys Monogr Ser. **215**, 277–290.
9. Borovsky J. E., and Valdivia J. A. (2018). The Earth's Magnetosphere: A Systems Science Overview and Assessment. *Surv Geophys*, **39(5)**, 817–859.
10. Milan, S. E., Clausen, L. B. N., Coxon, J. C., Carter J. A., Walach, M. T., Laundal K., Østgaard N., Tenfjord P., Reistad J., Snekvik K., Korth H. and Anderson B. J. (2017). Overview of Solar Wind–Magnetosphere–Ionosphere–Atmosphere Coupling and the Generation of Magnetospheric Currents. *Space Sci Rev* **206,** 547–573 (2017).
11. Dungey, J. W. (1961). Interplanetary magntic field and the auroral zones. *Physical Review Letters*, 6, 47-48.
12. Jankovicova, D., P. Dolinsky, F. Valach, and Z. Voros (2002), Neural network-based nonlinear prediction of magnetic storms, *J. Atmos. Sol. Terr. Phys.*, **64**(5-6), 651-656.
13. Anderson, B. J., S. I. Ohtani, H. Korth and A. Ukhorskiy (2005), Storm time dawn-dusk asymmetry of the large scale Birkeland currents, *J. Geophys. Res.*, **110**, A12220.

14. Shepherd, G. S. (2006). Polar cap potential saturation: Observations, theory, and modeling. *Journal of Atmospheric and Solar-Terrestrial Physics*, **69**, 234– 248.
15. Papitashvii, V. O., Rich, F. J., Heinemann, M. A., and Hairston, M. R. (1999). Parameterization of the Defense Meteorological Satellite Program ionospheric electrostatic potentials by the interplanetary magnetic field strength and direction *Journal of Geophysical Research,* **104**(A1), 177-184.
16. Pedatella, N. M., Forbes, J. M., & Richmond, A. D. (2011). Seasonal and longitudinal variations of the solar quiet (Sq) current system during solar minimum determined by CHAMP satellite magnetic field observations. *Journal of Geophysical Research*, **116**, A04317.
17. Chapagain, N. P. (2016), Equatorial ionospheric plasma drifts velocities using radar observations, *BIBECHANA*, **14**(2017), 1– 8: RCOST p.1.
18. Dal Lago, A., et al. (2006). The 17-22 October (1999) solar-interplanetary geomagnetic event: Very intense geomagnetic storm associated with a pressure balance interplanetary coronal mass ejection and a high speed stream, *J. Geophys. Res.*, **111**, A07S14.
19. Jian L. K., Russell, C. T., Luhmann, J. G. and Skoug R. M. (2006). Properties of Interplanetary Coronal Mass Ejections at One AU during 1995 – 2004, *Solar Physics*, **239**, 393-496.
20. Richardson I. G. and Cane H. (2010). Near-Earth Interplanetary Coronal Mass Ejections during Solar Cycle 23 (1996 – 2009): Catalog and Summary of Properties, *Solar Physics*, **264**(1), 189-237.
21. Chi Y., Shen C., Wang Y., Xu M., Ye P. and Wang S. (2016) Statistical Study of the Interplanetary Coronal Mass Ejections from 1995 to 2015, *Solar Phys*, **291**, 2419–2439.
22. West Jr., H. I., Buck, R. M, and Walton, J. R. (1972). Shadowing of electron azimuthal-drift motions near the noon magnetopause, *Nature Phys. Sci*., **240**, 6–7.
23. Kozyra J. U., Jordanova V. K., Horne R. B., and Thorne R. M. (1997). Modeling of the contribution of electromagnetic ion cyclotron (EMIC) waves to stormtime ring current erosion, in: Magnetic Storms, *Geophys. Mon. Ser*., **98**, 187–202.
24. Kozyra, J. U., Nagy, A. F., and Slater, D. W. (2006a). High-altitude energy source(s) for stable auroral red arcs, *Rev. Geophys*., **35**, 155–190.
25. Jordanova, V. K., Farrugia, C. J., Janoo, L., Quinn, J. M., Torbert, R. B., Ogilvie, K. W., and Belian, R. D. (1998). October 1995 magnetic cloud and accompanying storm activity: Ring current evolution, *J. Geophys. Res*., **103**, 79–92.
26. Daglis, I. A., Thorne, R. M., Baumjohann, W., and Orsini, S. (1999). The terrestrial ring current: origin, formation and decay, *Rev. Geophys*., **37**, 407–438.
27. Bargatze, L. F., Ogino, T., McPherron, R. L., & Walker, R. J. (1999). Solar wind magnetic field control of magnetospheric response delay and expansion phase onset timing. *Journal of Geophysical Research*, **104**, 14,583– 14,599.
28. Rostoker, G., Lam, H. L., & Hume, W. E. (1972). Response time of the magnetosphere to the interplanetary electric field. *Canadian Journal of Physics*, **50**, 544– 547.
29. Gonzalez, W. D., Josely, J. A., Kamide, Y., Korehi, H. W., Rostoker, G., Tsuruntani, B. T., & Vasylianas, V. M. (1994). What is a geomagnetic storm? *Journal of Geophysical Research*, **99**, 5771– 5792.
30. Gonzalez, W. D., & Tsurutani, B. T. (1987). Criteria of interplanetary parameters causing intense magnetic storm (Dst <−100 nT). *Planetary and Space Science*, **35**, 1101– 1109.

31. Adhikari, B., Dahal, S., Sapkota, N., Baruwal, P., Bhattarai, B., Khanal, K., & Chapagain, N. P. (2018). Field aligned current and polar cap potential and geomagnetic disturbances: A review of cross-correlation analysis. *Earth and Space Science*, **5**, 440– 455.
32. Wei, L. A., Fearing, M. A., Sternberg, E. J., & Inouye, S. K. (2008). The confusion assessment method: A systematic review of current usage. *Journal of the American Geriatrics Society*, **56**, 823– 830.
33. Akasofu, S.-I. (1978). Magnetospheric substorms. *Eos, Transactions American Geophysical Union*, **59(**2), 68– 73.
34. Knipp, D. J., Emery, B. A., Engebretson, M., Li, X., McAllister, A. H., Mukai, T., Kokubun, S., Reeves, G. D., Evans, D., Obara, T., Pi, X., Rosenberg, T., Weatherwax, A., McHarg, M. G., Chun, F., Mosely, K., Codrescu, M., Lanzerotti, L., Rich, F. J., Sharber, J., & Wilkinson, P. (1998). An overview of the early November 1993 geomagnetic storm. *Journal of Geophysical Research*, **103**, 26,197– 26,220.
35. Turner, N. E., Cramer, W. D., Earles, S. K., & Emery, B. A. (2009). Geoefficiency and energy partitioning in CIR-driven and CME-driven storms. *Journal of Atmospheric and Solar - Terrestrial Physics*, **71**, 1023– 1031.
36. Tenfjord, P., & Østgaard, N. (2013). Energy transfer and flow in the solar wind-magnetosphere-ionosphere system: A new coupling function. *Journal of Geophysical Research: Space Physics*, **118**, 5659– 5672.
37. Pulkkinen, T. I., Ganushkina, N. Y., Baker, D. N., Turner, N. E., Fennell, J. F., Roeder, J., Fritz, T. A. & Kettmann, G. (2001). Ring current ion composition during solar minimum and rising solar activity: Polar/CAMMICE/MICS results. *Journal of Geophysical Research: Space Physics*, *106*(A9), 19131-19147. doi: 10.1029/2000JA003036.
38. Østgaard, N., G. Germany, J. Stadsnes, and R. R. Vondrak (2002b), Energy analysis of substorms based on remote sensing techniques, solar wind measurements, and geomagnetic indices, *J. Geophys. Res.*, **107**, 1233, doi:10.1029/2001JA002002.
39. Stern, D. P. (1984), Energetics of the magnetosphere, *Space Sci. Rev.*, **39**(1-2), 193– 213, doi:10.1007/BF00173674.
40. Lu, G., Baker, D. N., McPherron, R. L., Farrugia, C. J., Lummerzheim, D., Ruohoniemi, J. M., Rich, F. J., Evans, D. S., Lepping, R. P., Brittnacher, M., Li, X., Greenwald, R., Sofko, G., Villain, J., Lester, M., Thayer, J., Moretto, T., Milling, D., Troshichev, O., Zaitzev, A., Odintzov, V., Makarov, G., & Hayashi, K. (1998). Global energy deposition during the January 1997 magnetic cloud event. *Journal of Geophysical Research*, **103**, 11,685– 11,694. https://doi.org/10.1029/98JA00897.